International Journal of
Molecular Sciences

MDPI

Article

A Murine Model of Glioblastoma Initiating Cells and Human Brain Organoid Xenograft for Photodynamic Therapy Testing

Alejandra Mosteiro [1,2,*,†], Diouldé Diao [1,†], Carmen Bedia [3], Leire Pedrosa [1], Gabriela Ailén Caballero [4,5], Iban Aldecoa [4,5], Mar Mallo [6], Francesc Solé [6], Ana Sevilla [7,8], Abel Ferrés [2], Gloria Cabrera [2], Marta Muñoz-Tudurí [9], Marc Centellas [9], Estela Pineda [10], Àngels Sierra Jiménez [1,11,*] and José Juan González Sánchez [1,2]

1 Laboratory of Experimental Oncological Neurosurgery, Neurosurgery Service, Hospital Clinic de Barcelona—FCRB, 08036 Barcelona, Spain; dioulde.dg@gmail.com (D.D.)
2 Department of Neurosurgery, Hospital Clínic de Barcelona, Universitat de Barcelona, 08036 Barcelona, Spain
3 Institute of Environmental Assessment and Water Research (IDAEA-CSIC), 08034 Barcelona, Spain; carmen.bedia@idaea.csic.es
4 Department of Pathology, Biomedical Diagnostic Center, Hospital Clínic of Barcelona, University of Barcelona, 08036 Barcelona, Spain; gailen@clinic.cat (G.A.C.); ialdecoa@clinic.cat (I.A.)
5 Neurological Tissue Bank of the Biobank, Institute of Biomedical Research August Pi i Sunyer (IDIBAPS), 08036 Barcelona, Spain
6 Microarrays Unit, Institut de Recerca Contra la Leucèmia Josep Carreras (IJC), ICO-Hospital Germans Trias i Pujol, Universitat Autònoma de Barcelona, 08916 Badalona, Spain; mmallo@carrerasresearch.org (M.M.); fsole@carrerasresearch.org (F.S.)
7 Institute of Biomedicine, University of Barcelona (IBUB), 08036 Barcelona, Spain
8 Department of Cell Biology, Physiology and Immunology, Faculty of Biology, Institute of Neuroscience, University of Barcelona, 08028 Barcelona, Spain
9 Laboratorios Gebro Pharma S.A., 08022 Barcelona, Spain; marc.centellas@gebro.es (M.C.)
10 Department of Oncology, Hospital Clinic de Barcelona—FCRB, 08036 Barcelona, Spain; epineda@clinic.cat
11 Department of Medicine and Life Sciences (MELIS), Faculty of Health and Live Sciences, Universitat Pompeu Fabra, 08036 Barcelona, Spain
* Correspondence: mosteiro@clinic.cat (A.M.); asierrajim@gmail.com (À.S.J.)
† These authors contributed equally to this work.

check for updates

Academic Editor: Giovanni Luca Gravina

Received: 13 July 2025
Revised: 19 August 2025
Accepted: 3 September 2025
Published: 12 September 2025

Citation: Mosteiro, A.; Diao, D.; Bedia, C.; Pedrosa, L.; Caballero, G.A.; Aldecoa, I.; Mallo, M.; Solé, F.; Sevilla, A.; Ferrés, A.; et al. A Murine Model of Glioblastoma Initiating Cells and Human Brain Organoid Xenograft for Photodynamic Therapy Testing. *Int. J. Mol. Sci.* **2025**, *26*, 8889. https://doi.org/10.3390/ijms26188889

Copyright: © 2025 by the authors. Licensee MDPI, Basel, Switzerland. This article is an open access article distributed under the terms and conditions of the Creative Commons Attribution (CC BY) license (https://creativecommons.org/licenses/by/4.0/).

Abstract

Glioblastoma (GB) is one of the most aggressive brain tumors, characterized by high infiltrative capacity that enables tumor cells to invade healthy brain tissue and evade complete surgical resection. This invasiveness contributes to resistance against conventional therapies and a high recurrence rate. Strategies capable of eliminating residual tumor cells are urgently needed. Photodynamic therapy (PDT) using 5-aminolevulinic acid (5-ALA), an FDA- and EMA-approved compound, induces selective accumulation of the photosensitizer protoporphyrin IX (PpIX) in metabolically active tumor cells, enabling targeted cytotoxicity through light activation. A major limitation to its clinical application is the unclear variation in the cytotoxic effect of PDT according to individual tumoral differences. In this study, we propose and validate an in vivo model of patient-derived GB initiating cells (GICs) and brain organoids to test the effects of PDT. First, patient-derived GICs were molecularly characterized by flow cytometry and copy number variation profiling using OncoScan CNV Assays, then co-cultured with human brain organoids to generate a hybrid model recapitulating key aspects of the tumor microenvironment. 5-ALA photodynamic therapy (PDT) efficacy was assessed in vitro by GFP-based viability measurements, LDH release assays, and TUNEL staining. Then, a murine model was generated to study PDT in vivo, based on a heterotopic (renal subcapsular engraftment) xenograft of the GICs-human brain organoid co-culture. PDT was tested in the model; in each subject, one kidney tumoral engraftment was treated and the contralateral served as a control. Immunofluorescence analysis was used to study the cell composition of the brain organoid-tumoral engraftment

after PDT, and the effects on non-GIC cells. The antitumoral effect was determined by the degree of cell death analysis with the TUNEL technique. The GICs-brain organoid co-culture resulted in tumoral growth and infiltration both in vitro and in vivo. The pattern of growth and infiltration varied according to the tumoral genetic profile. 5-ALA PDT resulted in a reduction in the number of GICs and an increase in apoptotic cells in all four lines tested in vitro. A correlation was found between the induced phototoxicity in vivo with the molecular typification of GICs cell lines in vitro. There were no changes in the number or distribution of neuronal cells after the application of PDT, while a reduction in active astrocytes was observed. 5-ALA PDT could be effective in eradicating GICs with a heterogeneous molecular profile. The hybrid human-murine model presented here could be useful in investigating adjuvant therapies in GB, under the concept of personalized medicine.

Keywords: glioblastoma; photodynamic therapy; 5-ALA; organoid; model

1. Introduction

Glioblastoma (GB) is the most common primary brain malignancy in adults, accounting for almost 80% of such tumors [1]. With the new 2021 World Health Organization Classification of Tumors of the Central Nervous System (CNS), molecular parameters have gained increasing relevance to define glioma subtypes [2,3], adding objectivity to diagnosis and improving patient stratification according to prognosis [4,5]. However, this implementation of tumor genetics has had little impact on the standard therapy for GB (Stupp protocol).

Unfortunately, recurrence is the norm, occurring on average seven months after treatment, invariably adopting a more aggressive form, and accounting for a one-year survival rate of approximately 60%. Notably, more than 80% of recurrences are located adjacent to the resection cavity. The fact that recurrences occur within the already treated area of resection denotes the ability of this tumor to resist conventional therapies. During the surgical resection, a certain degree of microscopic disease is left inadvertently; this is thought to correspond to the tumor front infiltrating white matter tracts and small vessels [6–8]. Several months after the surgery, this microscopic disease would be responsible for the tumoral recurrence due to senescence-induced changes after radiotherapy [9,10]. Thus, to prevent tumor recurrence, a plausible solution would be a tumor-selective locally delivered therapy, able to eliminate the microscopic disease left after surgical resection but avoiding damage to non-tumoral cells of the surrounding brain.

To serve this idea, photodynamic therapy (PDT) has been proposed. Indeed, after 5-aminolevulinic acid (5-ALA) administration, GB cells accumulate protoporphyrin IX (PpIX), a molecule that acts both as a fluorophore and a photosensitizer (PS). PpIX fluorescence can be visualized using a modified neurosurgical microscope and is already used for photodynamic diagnosis (PDD) [11,12].

5-ALA already represents a standard approach for intraoperative fluorescence-guided oncologic neurosurgery. Exploiting 5-ALA as both a fluorophore and a PS to visually identify the neoplastic tissue and, simultaneously, to selectively destroy it, could improve the success of GB treatment [13]. This synergistic mechanism of action, which integrates both therapeutic and diagnostic capabilities into one single product, has shown exciting prospects [14].

Although promising, data on the photo-toxic effects according to the diversity of genetic subtypes in GB is scarce [15]. Therefore, an experimental model to evaluate the tumor-sensitivity to the therapy is needed. Ideally, this model should mimic both the heterogeneity of the human GB and the interrelation with the brain-tumor microenvironment.

Our group has recently reported that glioblastoma initiating cells (GICs) co-cultured with brain organoids recapitulate many aspects of the disease and can be used in vitro to assess both the efficacy of local therapies and collateral damage to the surrounding brain cells [16]. The aim of the current study is to extrapolate this GIC-organoid co-culture into an in vivo murine model, in which to characterize the efficacy of PDT according to the genetic profile of GICs.

2. Results

2.1. Patient-Derived HCB-GICs Malignant Phenotype

Samples from patients operated on in the Hospital Clinic of Barcelona (HCB) were used to obtain HCB-GICs (Supplementary Table S1). All four selected patients were diagnosed with MGMT-methylated IDH wild-type grade 4 gliomas, following the WHO Classification of Tumors of the Central Nervous System criteria [2] by the Pathology Department. Mean age was 60.75 ± 11.44 years, with an equal distribution of 2 men and 2 women. Clinical details can be found in Supplementary Materials. Progression-free survival (PFS) intervals varied widely between the four subjects, from early progression (95 days) to prolonged intervals (795 days).

Four different HCB-GICs (Figure 1A) were obtained from the patients' samples: HCB-GIC1, HCB-GIC4, HCB-GIC19 and HCB-GIC20, with similar growth ratios but differing in their phenotype. After 15–20 days of isolation, HCB-GIC1, HCB-GIC19 and HCB-GIC20 formed tumorspheres, in contrast to HCB-GIC4, which grew in adhesion with a characteristic spicular cytoplasmic neural-like extension (Figure 1B and Supplementary Figure S1). The stemness and invasive nature were further proven by evaluating the expression of specific markers (CD133 and CD44, respectively) with flow cytometry.

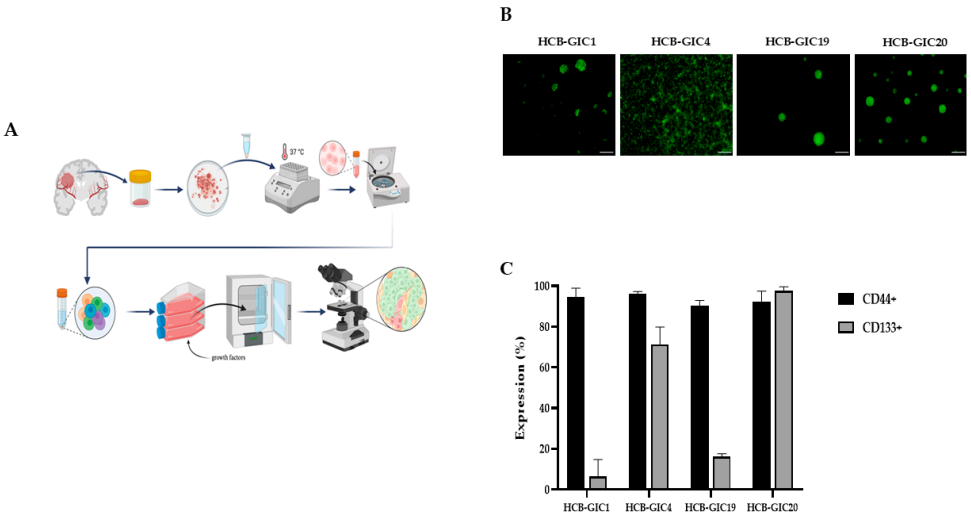

Figure 1. Establishment of Primary Human Glioblastoma tumorosphere cultures from biopsies. (**A**) Isolation protocol of HCB-GICs from human tissue samples. Schematic protocol to set up primary glioblastoma initiating cell (GICs) cultures. It includes steps from surgical human tissue samples until follow-up maintenance of GICs, as indicated in the scheme. (**B**) Four HCB-GICs were obtained: HCB-GIC1, HCB-GIC4, HCB-GIC19 and HCB-GIC20. Cultures of HCB-GICs constitutively expressing GFP are shown on maintenance conditions with complete NSC medium. (**C**) Flow cytometry analysis of CD133 and CD44 expression. HCB-GICs cells transfected with green fluorescent protein (GFP) were stained with anti-CD133 phycoerythrin (PE) or anti-CD44 labeled with AF594 as a secondary and subjected to flow cytometer analysis, collecting 10,000 events. Samples were analyzed on a Fortessa 5L flow cytometer. The figure is representative of three independent experiments. ANOVA test was performed to compare GFP+CD44+ (light gray bars) and GFP+CD133+ (dark gray bars) expression between the four cell lines. The results show that there are significant differences in CD133 expression between the cell lines, but not in CD44 expression.

CD133 showed variable expression among HCB-GICs (Figure 1C). Whereas <20% of cells were CD133+ in HCB-GIC1 and HCB-GIC19, >70% of HCB-GIC4 and HCB-GIC20 cells were CD133+ ($p < 0.0001$). With 90% of cells across all four HCB-GICs being CD44+, no significant differences in CD44 expression were observed ($p = 0.384$) (Figure 1C). These findings confirmed that the aggressive phenotype is not always associated with the CD133 stem cell marker.

2.2. Patient-Derived HCB-GICs Genotype

We first explored the similarity between HCB-GICs obtained by primary culture of GB biopsies and their original tumor, to assess any deviation that could occur during the process of in vitro obtaining and expanding HCB-GICs (Supplementary Figure S2). Shared imbalances were evaluated for their dimension (base pair length) and their representativeness (mosaicism percentage).

The comparison between DNA from the tumor tissue and the DNA from the HCH-GICs showed that HCB-GIC4, HCB-GIC19 and HCB-GIC20 shared almost 100% similarity. Interestingly, HCB-GIC1, the only one that differed from its primary tumor, had the highest accumulation of genetic alterations, suggesting genomic instability prone to induce in vitro genetic changes, resulting in the highest copy number alterations (CNA).

We looked for the three main canonical pathways described as being involved in glioma genesis and altered in high-grade gliomas: p53, Rb and PIK3KC A loss in p53 was seen in HCB-GIC1, and preserved in HCB-GIC4, HCB-GIC19 and HCB-GIC20 cells. CNA of HCB-GICs confirmed that only HCB-GIC1 had gains in both tumor suppressor genes, p53 and Rb, validating the clinicopathological diagnosis of the tumor samples. Since p53 pathway is more often modulated by several factors, including the upstream microtube-binding protein regulators as MDM1 and MDM2 [17], we checked if these genes were altered. However, our analysis indicated that both MDM1 and MDM2 remained normal.

HCB-GIC1 and HCB-GIC4 showed lost Rb; therefore, we examined genes such as CDK4 and CDK6, CDKN2A/B and CCND2 from Rb pathways. We found gains on CDK6 in all HCB-GICs with CDKN2 losses, while CDK4 and CCND2 gains were only observed in HCB-GIC1.

PIK3KC amplifications were found in HCB-GIC1, and PIK3KC was lost in HCB-GIC4. The PIK3KC pathway was further studied, including PIK3CA, PIK3R, PTEN, EGFR, PDGFR1 and NF1. HCB-GICs had exhibited PTEN losses, which were biallelic in HCB-GIC4 and HCB-GIC19. In addition, all HCB-GICs had EGFR amplifications, the highest 12 copies in HCB-GIC20. Moreover, PIK3CA and PIK3R were both amplified in HCB-GIC1. PDGFR1 was amplified in HCB-GIC1, lost in HCB-GIC4 and normal in both HCB-GIC19 and HCB-GIC20. NF1 was normal in all cases, except for HCB-GIC1, where the original tumor sample presented cnLOH loss, in mosaicism, whereas the GIC-derived showed only loss.

A genotypic heterogeneity among the four HCB-GICs was evident in the microarray analysis (Supplementary Figure S3). HCB-GIC1 exhibited the highest number of alterations accumulated in the three main pathways, with 20 altered genes, followed by HCB-GIC4, with 10, and HCB-GIC19 and HCB-GIC20, both with 6 altered genes.

2.3. Organoid Cell Composition and HCB-GICs Differential Phenotype Determined Their Growth on Cerebral Organoid Co-Cultures

The expression of TUJ1 (neurons), GFAP (astrocytes), SOX2 (neural progenitor cells), and O4 (oligodendrocytes) in the brain organoids used in this study had been previously characterized and validated by immunofluorescence in our published work. That study demonstrated that these organoids reliably develop the main cell types found in neural tissue [16].

The pluripotent stem cell line BJ-Sev-iPSC possesses the intrinsic ability to self-organize into brain-like structures following sequential media changes. At 43 days, the multicellular aggregates contained polarized neural progenitors mimicking the developing cortex, as confirmed by the expression of key neural markers (Supplementary Figure S4).

The pluripotent stem cell line BJ-Sev-iPSC owned the intrinsic ability to self-organize into brain-like structures after subsequent changes of media. At 43 days, the multicellular aggregate contained a group of polarized neural progenitors mimicking the developing cortex, with cells expressing neural, stem and glial cell markers. Immunofluorescence analysis on cryosection organoids confirmed the expression of Tubulin betta class 3 (TUBB3-TUJ1), a marker of neurons at an early stage of differentiation, and glial fibrillary acidic protein (GFAP), an astrocyte-specific marker (Supplementary Figure S4). These validated brain organoids were subsequently used to establish HCB-GICs co-cultures.

HCB-GICs' ability to infiltrate organoids was assessed after 30 days of co-culture to identify the depth of GFP-positive cells migration (Figure 2B). All HCB-GICs showed successful engraftment, with GFP+ cells growing within the organoid more than 100 µm from the surface, indicating the aggressiveness of the migration and invasion process (Figure 2A and Supplementary Figure S5). The four HCB-GICs had different invasion features, with HCB-GIC1, HCB-GIC19 and HCB-GIC20 forming tumorspheres, and HCB-GIC4 disseminated within the organoid and triggering the characteristic spicular cytoplasmic neural-like extensions.

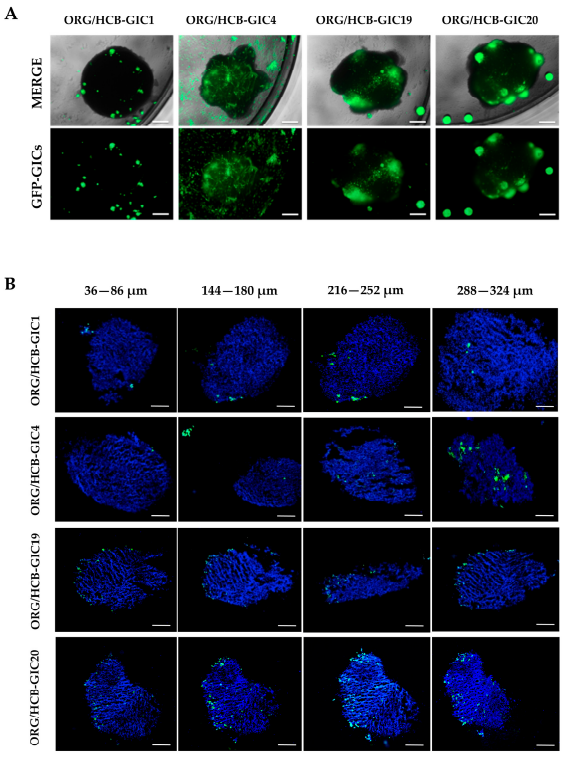

Figure 2. Start and progression of HCB-GICs and brain organoids co-culture. (**A**) Co-cultures were initiated on a 47-day-old brain organoid using 2×10^3 cells per cell line. The experimental outline at 14 days post-initiation shows GFP-GIC infiltration (green fluorescence) patterns within the brain organoids (dark mass). HCB-GIC1, HCB-GIC19 and HCB-GIC20 have similar invasive disposition, but HCB-GIC4 show different behavior with characteristic spicular cytoplasmic neural-like extensions. Scale bars are: 100 µm. (**B**) HCB-GICs infiltrate brain organoids after 30 days of culture (N = 1 sample per condition). Fixed tissues were sliced at 12 µm. Nikon Eclipse Ni micrographs visualizing invasion of consecutive slides of frozen HCB-GIC organoid co-cultures show invasive GFP+ cells infiltrating the minibrain at indicated depths in the four models studied. Nuclei are counterstained with DAPI (blue). Scale bars are 100 µm.

Moreover, we evaluated other malignant-associated phenotypic markers (Supplementary Figure S7A), the expression of vimentin and nestin proteins was analyzed [18]. Vimentin and nestin were generally expressed by the four HCB-GICs growing in brain organoids. The expression of SOX2 was analyzed in HCB-GIC co-cultures and detected in the four types, located mainly on tumoral foci. These results indicate that a stable malignant phenotype is maintained in the HCB-GICs co-cultured with brain organoids.

2.4. Photodynamic Therapy Effects In Vitro: HCB-GICs Infiltrating Brain Organoids

After 5-ALA PDT in vitro, a significant decrease in the GFP fluorescence between the irradiated and non-irradiated co-cultures of HCB-GIC1, HCB-GIC4 and HCB-GIC19 was observed after 24 h and 72 h, ranging between 0.4 and 0.6-fold decrease ($p = 2.4 \times 10^{-3}$, $p = 5.3 \times 10^{-4}$, and $p = 2.1 \times 10^{-4}$, respectively, at 24 h; $p = 5.1 \times 10^{-3}$, $p = 1.5 \times 10^{-4}$, and $p = 1.5 \times 10^{-3}$, respectively, at 72 h). In HCB-GIC20 co-cultures, a decreasing pattern in the fluorescence levels was also observed, although not statistically significant even 72 h after irradiation (Figure 3A,B and Supplementary Figure S6).

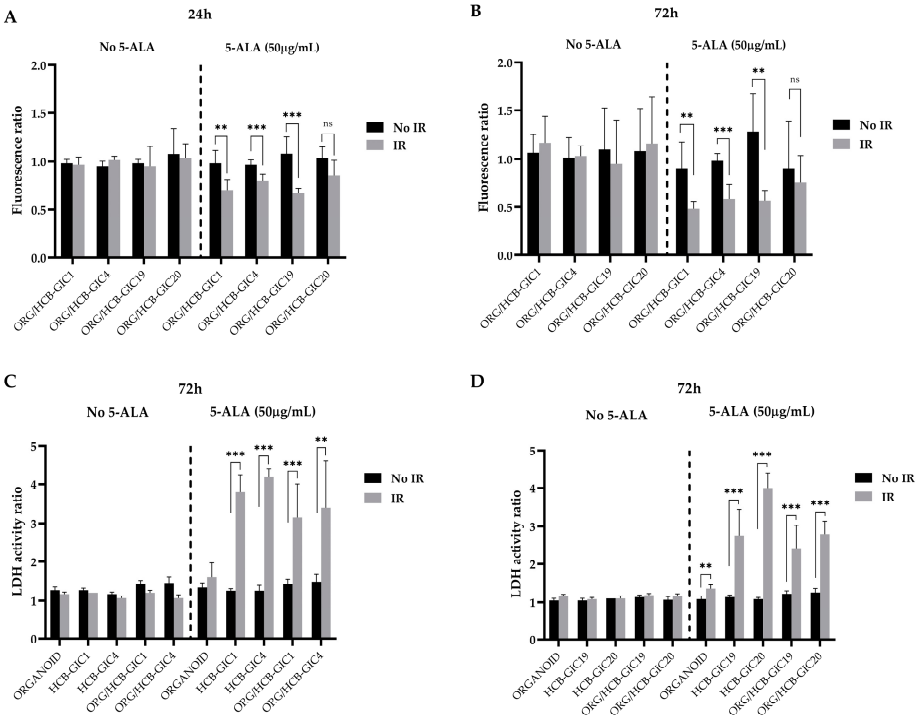

Figure 3. Photodynamic therapy in HCB-GICs infiltrating brain organoids. Two paired 96-well plates were used—one non-irradiated and one irradiated—with each plate split into two halves: medium alone and 5-ALA treatment (50 µg/mL). Each condition was performed in six replicates per column. GFP fluorescence ratios of HCB-GICs infiltrating organoids were calculated by dividing the fluorescence at 24 h (**A**) and 72 h (**B**) by the fluorescence measured immediately post-irradiation. Panels C and D show LDH assay results on supernatants collected 72 h after irradiation for HCB-GIC1 and HCB-GIC4 (**C**) and HCB-GIC19 and HCB-GIC20 (**D**). Statistical significance was determined by Holm–Sidak multiple comparisons test with ** $p < 0.01$, *** $p < 0.001$, ns (no statistical differences). See Discussion, Section 2.4 for detailed statistical analysis.

A significant increase in cell death ratios was detected in the wells treated with 5ALA/PDT, as shown by LDH assay analysis (Figure 3C,D), compared to their untreated counterparts (Supplementary Figure S6) after 72 h, in both HCB-GICs alone and those infiltrating organoids (HCB-GIC1, $p < 1 \times 10^{-6}$ and 6.2×10^{-4}; HCB-GIC4, $p < 1 \times 10^{-6}$ and 3.5×10^{-3}; HCB-GIC19, $p = 1.5 \times 10^{-4}$ and $p = 5.6 \times 10^{-4}$; HCB-GIC-20, $p < 1 \times 10^{-6}$ and $p < 1 \times 10^{-6}$). In wells containing only organoids, no increase in cell death was observed.

This pattern was confirmed by immunofluorescence, which revealed a visible reduction in fluorescent cells in HCB-GICs co-cultured organoids after PDT compared to non-treated controls (Figure 4A). Similarly, cell death analysis using TUNEL staining demonstrated a reduction in HCB-GICs accompanied by increased apoptotic signals after PDT in all four co-culture systems (Figure 4C).

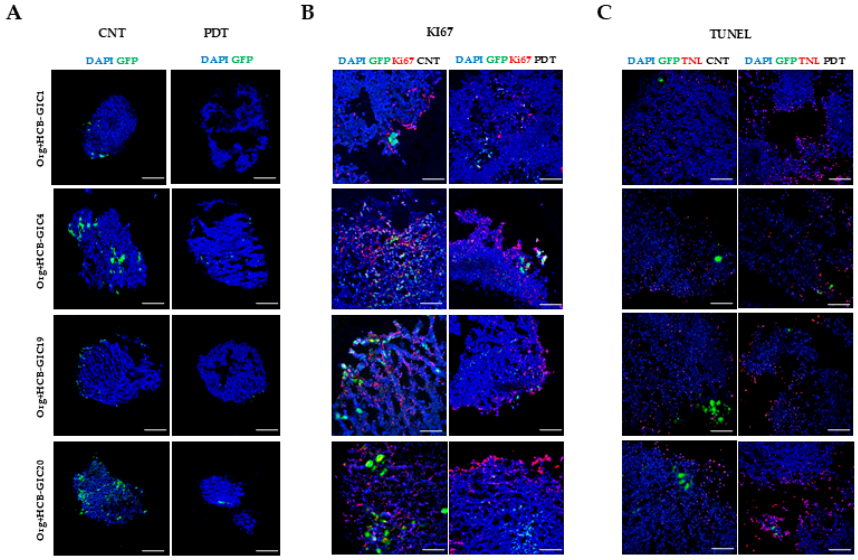

Figure 4. Immunofluorescence analysis of proliferation (Ki-67) and apoptosis (TUNEL) in PDT-treated co-cultures. Co-cultures were fixed at 30 days and cryosectioned at 12 µm (one section per condition) for qualitative immunofluorescence. HCB-GICs expressing GFP (green) invaded brain organoids and were divided into two groups: pretreated with 5-ALA (50 µg/mL) prior to PDT and untreated (control). Panels A–C show representative sections: (**A**) illustrates GFP^+ GIC distribution in control and PDT-treated organoids (scale bars: 100 µm). (**B**) Panel B displays Ki-67 immunostaining (red) with DAPI counterstain (blue), comparing untreated controls (left) to PDT-treated samples (right) (scale bars: 20 µm). (**C**) Panel C shows TUNEL staining (red) under the same layout. PDT reduced Ki-67^+ nuclei and increased $TUNEL^+$ nuclei relative to controls. Images were acquired on a Nikon Eclipse Ni microscope and processed with ImageJ 1.54g. Color legend: Blue, DAPI (4′,6-diamidino-2-phenylindole); green, GFP (green fluorescent protein); red, ki67; black, PDT (photodynamic therapy).

Regarding tumor capacity to grow, infiltrate and resist apoptosis after PDT, we assessed the expression of vimentin, nestin and SOX2 by immunofluorescence. While the first two appeared unchanged after therapy, SOX2 expression showed an apparent decrease after irradiation (Supplementary Figure S7).

2.5. Photodynamic Therapy Effects In Vivo: HCB-GICs-Brain-Organoid Xenografts

HCB-GIC20 and HCB-GIC1 infiltrating brain organoids (15 days of in vitro co-culture) were xenografted in the renal subcapsular space of both NSG mice kidneys (N = 3 in each group). Tumor and organoid neural tissue expansion were evaluated 40 days after engraftment.

PDT effectively decreased the HCB-GIC20 tumoral burden, measured as relative fluorescent units (RFU) on treated kidneys compared to contralateral untreated controls ($p = 0.01$) (Figure 5A,B). PDT proved to be effective even in cases of a big tumoral mass. Similar results were obtained with HCB-GIC1 tumors, where the average tumor RFU from control kidneys compared to that from treated kidneys was significantly different ($p = 0.0483$) (Supplementary Figure S10).

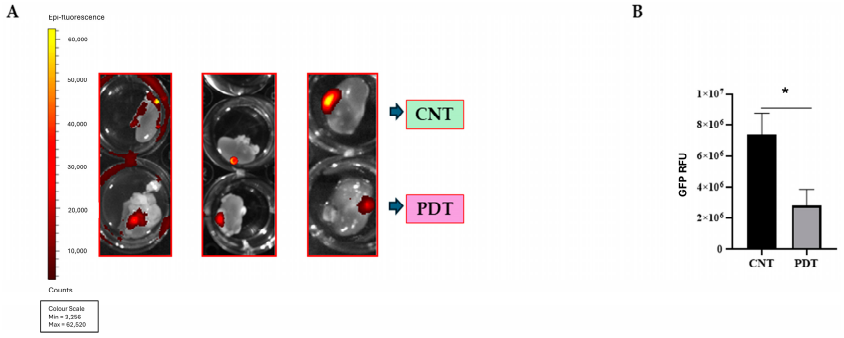

Figure 5. Ex vivo PDT efficacy in HCB-GIC20 organoid engraftment (N = 3 mice). Each mouse received two contralateral kidney implants: one control and one treated with PDT. At the endpoint, kidneys were harvested, and GFP fluorescence was measured ex vivo on an IVIS Imaging System (Caliper) to assess tumor burden. RFU values were corrected for local background and normalized to the number of implanted organoids. (**A**) Representative IVIS images of control (top row) and PDT-treated (bottom row) kidneys; the heatmap scale indicates RFU intensity. (**B**) Quantification of normalized GFP RFU in control versus PDT-treated kidneys. Data are mean ± SEM; unpaired two-tailed *t*-test performed in GraphPad Prism 8.0.2 on Fiji-processed images, * $p = 0.0104$.

Cell death was analyzed with the TUNEL technique (Figure 6A), which confirmed a statistically significant increase in apoptotic nuclei in treated cases, compared to untreated controls ($p = 0.0371$) (Figure 6B). The positive apoptotic nuclei were located within the necrotic areas.

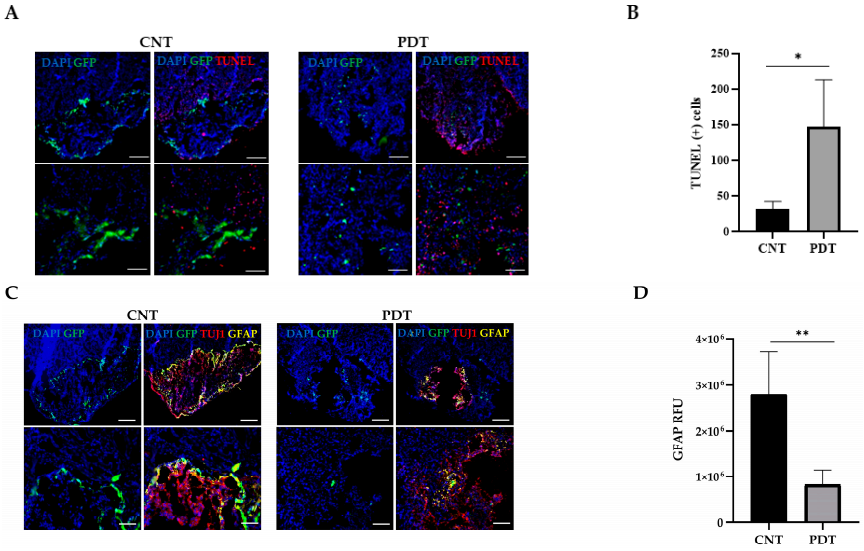

Figure 6. Immunofluorescence analysis of neuronal, glial, and apoptotic markers in HCB-GICs organoid grafts. Co-cultures were implanted into contralateral kidneys, with one kidney serving as an untreated control and the other subjected to PDT. (**A**) TUNEL staining (red) and GFP$^+$ tumor cells (green) in HCB-GIC20 organoid grafts with DAPI counterstain (blue). Sections from untreated control kidneys show sparse apoptotic nuclei at the tumor periphery, while PDT-treated kidneys exhibit a marked increase in TUNEL$^+$ nuclei coinciding with reduced GFP$^+$ tumor density. Scale bars: 100 µm and 20 µm. (**B**) Quantification of TUNEL$^+$ nuclei in five random 40× fields per sample (N = 3 mice) revealed a significant increase after PDT (unpaired two-tailed *t*-test performed in GraphPad Prism on Fiji-processed images, $p = 0.0371$). (**C**) TUJ1 (neurons, red) and GFAP (astrocytes, yellow) immunofluorescence with GFP$^+$ tumor cells (green) and DAPI (blue). In controls, GFP$^+$ cells infiltrate the organoid, TUJ1$^+$ neurons outline its structure, and GFAP$^+$ astrocytes are interspersed within and at the invasive front. PDT treatment markedly reduces GFP$^+$ infiltration and GFAP$^+$ astrocyte presence. Scale bars: 100 µm and 20 µm. (**D**) Quantification of GFAP$^+$ area in five random 40× fields per sample (N = 3 mice) showed a significant decrease after PDT (unpaired two-tailed *t*-test performed in GraphPad Prism on Fiji-processed images, $p = 0.0071$; * $p < 0.05$, ** $p < 0.01$). Color legend: Blue, DAPI (4′,6-diamidino-2-phenylindole); green, GFP (green fluorescent protein); red, TUJ1 (beta-tubulin III), yellow, GFAP (Glial fibrillary acidic protein).

To determine potential effects of PDT on the surrounding brain cells, the expression of neural (TUJ1) and astrocytes (GFAP) was analyzed in the engrafted kidneys by IF (Figure 6C,D). GFP indicative of tumor cells appeared surrounding necrotic areas, which were compatible with remaining brain organoid cells, where positive TUJ1 neurons are located. GFAP+ cells were observed in two different locations, in the middle of the necrotic areas and in the periphery of these areas, in close relation with tumor cells, suggesting reactive astrocytes. The quantity of these GFAP+ cells surrounding tumor cells diminished in the treated cases compared to untreated controls ($p = 0.0071$). GFAP+ cells were identified as astrocytes and not tumoral cells, as they did not express GFP.

3. Discussion

In this translational study, we evaluate the effects of 5-ALA-mediated PDT in an unprecedented experimental design of human glioblastoma, based on a co-culture of patient-derived HCB-GICs and human brain organoids, both in vitro and in an in vivo murine model. HCB-GICs were obtained from a series of patients operated on in our institution, demonstrating the potential of the model to study treatment effects under the concept of personalized medicine. According to our data, PDT seems effective both in vitro and in vivo. Moreover, the variations seen in the tumor cytotoxic effect according to the intrinsic genetic profile of each HCB-GIC subtype can be reproduced under in vivo conditions. The present design could be used to optimize preclinical studies of PDT and to explore adjuvant strategies to enhance 5-ALA phototherapeutic and photodiagnostic effects in gliomas.

3.1. A New Concept in GB Preclinical Investigation Models

Over the years, evidence generated by our laboratory and others has shown that patient-derived GICs are the most biologically and phenotypically relevant cells to study GB tumor initiation, maintenance and invasion [19]. The capacity for self-renewal and multi-lineage differentiation of GICs drives the increased resistance to ionizing radiation and cytotoxic drugs, limiting the effectiveness of current GB treatments [20]. The use of HCB-GICs for the development of tumor spheroids co-cultured with human brain organoids has provided a unique platform to characterize the behavior of GB, understand its relations with the tumor microenvironment, and test new therapies [21].

The introduction of organoids and tumorspheres as 3D models has enabled us to recapitulate more accurately the heterogeneity of the brain tissue and tumor properties [22]. These 3D constructions are obtained by culturing pluripotent stem cells in specific mediums that promote cell differentiation, and by subsequently co-culturing them with tumoral cells or spheres. Yet, they lack vascularization and are not able to recapitulate the systemic responses to tumor development and treatment regimes.

To overcome some of these limitations, we used a three-stage strategy to develop a valid model for evaluating the effects of PDT in GB. First, we obtained and characterized HCB-GICs from patients who had been operated on for GB. Second, we used these human HCB-GICs cell lines to infiltrate human brain organoids, containing neural, stem and glial cells. This 3D culture of HCB-GICs and brain organoids served as a platform to profile the malignant behavior of the different HCB-GIC subtypes, and to test their response to PDT with 5-ALA. Third, we transferred the HCB-GICs-organoid co-culture to the renal subcapsular space of NSG mice to test PDT in vivo.

We optimized the primary culture protocol, ensuring the maintenance of the initial HCB-GICs phenotype. The striking ability of HCB-GFP-GICs to proliferate and infiltrate the cerebral organoid simulated the infiltrative phenotype of GB. This cellular framework provided a potential mechanism for cell–to–cell signaling and intrinsic secretion of growth

factors, guiding neuronal and glial development, altogether supplying a perfect microenvironment for HCB-GICs to invade and infiltrate organoids.

Only one of the cell lines showed significant genetic deviations from the original tumor, the HCB-GIC1. This underscores that the heterogeneity of GB might induce a sampling to in vitro disaggregation with different subpopulations, even with some advantageous cells able to develop subclones expanding the main genetic alteration and giving value to the model for research purposes.

3.2. Profiling Patient-Specific HCB-GIC Cell Lines

During the first stage of characterization of HCB-GICs derived from patients with GB, we found several differences in the genetic and molecular profiles. According to the consensus clustering that identifies four subtypes of GB, a high level of EGFR amplification is observed in 97% of the classical subtype and infrequently in other subtypes of GB [23]. EGFR amplification was found mainly in our HCB-GIC20 cell line. Deletions of NF1 with an altered Akt pathway, which characterizes the mesenchymal subtype, were found in our HCB-GIC1 line. Losses of PDGFR1, which are typical in the proneural subtype, were found in our HCB-GIC4 line.

CD133 is a membrane-bound glycoprotein seen on the surface of stem cells, used as a biomarker for GICs. CD133 is associated with the mesenchymal phenotype of GB cells, with poor prognosis, therapy resistance, and tumor recurrence [24]. We found CD133+ cells expressed mainly in the HCB-GIC4 and HCP-GIC20 lines. CD133 has been associated with the ability of tumor cells to self-renew and to grow in the form of aggregates (tumorspheres) in vitro [24]. In our sample, both CD133+ and CD133− cells were capable of forming tumorspheres, except for HCB-GIC4, which, despite being CD133+, did not demonstrate tumorsphere-forming ability and instead grew primarily in adherent conditions.

All HCB-GICs overexpressed CD44, which has been associated with the activation of genes mediating cell invasion under severe hypoxia conditions, and with genes mediating cell proliferation under moderate hypoxia. Both genetically activated pathways are key components of GB recurrence [25]. Our HCB-GIC cells also expressed the "stemness" markers Nestin, Vimentin and SOX2, which are known contributors to the invasiveness and infiltrative behavior of GB, and which allowed the tumorspheres to invade brain organoids.

3.3. Evaluating 5-ALA PDT Effect on HCB-GICs-Organoid In Vitro Model

Our group had previously explored the effects of 5-ALA-mediated PDT in vitro in a platform of GICs infiltrating cerebral organoids. In this initial experience, we demonstrated that two different GB cells, GIC7 and PG88, had different capacities to invade the brain organoid, and showed a different response to PDT [16].

At this stage, we used this model to test the effects of PDT in a series of HCB-GICs derived from patients operated on for GB. Here, we demonstrate that patient-derived HCB-GICs can invade the brain organoids and, importantly, remain susceptible to PDT. After the HCB-GICs-organoids were exposed to a medium containing 5-ALA and subsequently brought to a light source of 485 nm and 1.2 J/cm^2, the burden of tumor cells in the organoids significantly decreased, while the cell death markers significantly increased.

Our findings support the idea that 5-ALA-mediated PDT can be an effective therapy for treating GB cells within the tumor niche. The model thus created could also be explored to study the potential adverse effects of PDT on the normal surrounding brain cells within the organoid. However, a limitation in this scenario is the lack of vascularization of the brain organoid. Indeed, the ability of GB to invade and induce the formation of neo vessels is a primary characteristic of this tumor [8]. This limitation may be overcome with an in vivo engraftment.

3.4. Evaluating 5-ALA PDT Effect on HCB-GICs-Organoid In Vivo Model

To better understand the limitations of the GICs-organoid in vitro model, we transferred the HCB-GICs co-cultured with human brain organoid to an experimental in vivo murine model. The spherical co-cultures of human GICs-organoids were implanted in the renal subcapsular space of immunosuppressed NSG mice [26]. This allowed us to observe the behavior and growth of the GICs-organoid in a vascularized environment. The design revealed a powerful in vivo system to recapitulate many aspects of GB development.

Compared to other murine models of GB, the unique content of both tumor cells and normal brain cells, both belonging to humans, makes this a unique platform. As both GB and neural/glial cells coexist within the same culture, it allows observing the interactions between transformed and non-transformed cells, making it useful to study essential tumor biology and giving valuable information for preclinical investigation of new compounds. For drug screening, this design enables an analysis of anti-tumor effects accompanied by collateral effects on healthy neural tissue, all in the same platform.

Optimizing PDT effects can be undertaken by increasing 5-ALA uptake, PpIX accumulation or exploring different light irradiation regimens that affect tissue oxygenation and may influence free radical production and oxidative stress. The importance of fractionation has already been emphasized by Curnow et al. and Vermandel et al. [27,28]. They found that the level of tissue oxygen at the treatment site was affected by the light regimens and that this indeed affected treatment effects. In our study, we opted for a rather simple irradiation scheme, as the main objective was to validate a model based on the combination of patient-derived GICs and human-derived glioneuronal organoids in which to test PDT. However, based on our encouraging findings, future experiments are warranted in which the effects of fractionated irradiation, controlled hyperoxygenation, or variable fractionated schemes based on PtiO2 values can be tested.

3.5. Strengths and Limitations of the GICs-Organoid Xenograft Model

In vivo models represent a step forward in modeling tumor complexity, as cells are implanted in a living organism where many types of dynamic interactions may occur, which condition therapy effectiveness. These may overcome some of the limitations seen in in vitro organoid models, in which the microenvironment interactions are restricted to cells that are already present in the tumor or that are artificially reconstructed and maintained by adding high amounts (even non-physiological) of cytokines, growth factors, serum, nutrients, etc.

An important feature in the HCB-GICs-organoid xenograft in mice is that tumoral and glioneural cells derive from humans and can be personalized with patient-derived tumoral and peripheral pluripotent cells. This advantage may be exploited to test the effects of specific therapies before administering them to the patient. Another remarkable asset of working with hybrid in vivo models based on organoid engraftment is the presence of vascularization and systemic immune responses, which may provide additional information regarding treatment response and mechanisms of resistance.

The limitations of this model are inherent to its xenograft nature and to its heterotopic location. The engraftment of human cells in mice requires the use of immunosuppressed strains, which do not allow studying the systemic immune responses to tumor development and to treatment. Conversely, it allows the use of patient-specific cells, which could have potential benefits in testing therapeutic responses in the era of personalized medicine. Furthermore, the idea of placing the tumor-organoid engraftment in the kidney allowed simplifying and homogenizing the experimental procedure and transforming the avascular tumor-organoid platform into a vascular one. However, this construction does not allow

accounting for specific intracranial phenomena, such as the effects of the blood-brain barrier in the treatment response.

3.6. Immunological Implications of 5-ALA PDT Therapy

Recent studies have demonstrated that tumor-associated myeloid cells, particularly hyperactivated macrophages, exhibit elevated expression of heme oxygenase-1 and play a key role in ALA metabolism. These cells can accumulate and convert ALA into PpIX, suggesting a strong immunological and cellular component to PDT sensitivity and toxicity [29,30].

Although we did not specifically study myeloid cells in this study, we did find changes suggestive of immunological effects secondary to 5-ALA-mediated PDT. GFAP+ cells (astrocytes) were seen in the areas of infiltrative tumor. This astroglial proliferation/migration might be attributed to differences in the tumor microenvironment that promote astrocyte interactions with glioma cells and seem essential for glioma development and a crucial target in preventing glioma recurrences [16,31]. The role of astrocytes may change in the presence of a glial tumor [32]. Indeed, a distinct "reactive type" of astrocyte has been found in tumors, different from astrocytes purified from non-malignant specimens. This astrocytic change may be responsible for the impairment of immune responses, inducing a low reaction to novel therapies targeting the GB microenvironment [33]. The ability of astrocytes to survive local therapies is of particular interest, since they might mediate the antitumorigenic effect of these therapies and the potential collateral damage to the surrounding brain tissue [34].

In that sense, in our model, PDT decreased GFAP+ cells as well as HCB-GICs but did not seem to affect other glial and neural cells present in the organoid. These observations may indicate the relative specificity of the PDT treatment for both tumor and reactive astrocytes, while preserving the normal brain.

The modulation of the immunological response in the tumor microenvironment may explain the fact that PDT anti-tumoral effects seemed to be potentiated in vivo. In fact, the degree of tumor fluorescence in HCB-GIC20 cells was significantly higher in the in vivo xenograft than in the in vitro application of PDT. Following these preliminary observations, the presence of myeloid or other stromal components in the tumor microenvironment warrants further investigation in our model.

All in all, a major strength of this model, including human-derived glioneural organoids, is its potential ability to test collateral effects of damage to the surrounding brain when applying direct therapies such as 5ALA-mediated PDT in gliomas. Based on our preliminary findings, after the application of PDT, the number of TUT+ cells (corresponding to neurons) remained unchanged, while the GFAP+ cells (considered as reactive astrocytes) diminished in the area surrounding the tumor. These observations support the idea of PDT as tumor-specific and, up to some extent, immunomodulatory, yet this idea warrants future detailed exploration.

3.7. Limitations of the Study

Several limitations can be found in this study. First, the fact that the GIC cell lines derived from patient-specific samples limits the extrapolation of the therapeutic effects to the general population. Second, the therapeutic scheme for PDT in terms of irradiation time and dosage has not been standardized, and different results may be obtained with other regimes. Third, the effects attributed to the intracranial space, such as the presence of the blood–brain barrier or raised intracranial pressure, cannot be accounted for in this model. Fourth, the specific design in this study, where animal sacrifice was performed at the final stage after therapy, did not allow for a formal comparison of tumor volumes between the treatment and control kidney engraftments. However, given that the same

number of GIC-organoids were implanted in each kidney and that they were exposed to the same conditions, a parallel tumor growth shall be assumed.

4. Materials and Methods

4.1. Obtention of Glioblastoma Cell Lines and Organoids

Glioblastoma-initiating cells (GICs) were obtained from surgical biopsies at the Hospital Clínic of Barcelona, as previously described by Frenster et al. (2018) [35]. All human-derived samples were collected with written informed consent under approval from the institutional Ethics Committee and in compliance with European and national biomedical research regulations. Detailed laboratory methods are provided in the Supplementary Materials.

Cells transduction and Organoid generation. For longitudinal tracking, HCB-GICs were transduced with GFP-expressing lentiviral vectors [36]. Human iPSC-derived cerebral organoids were generated over 47 days in defined spheroid media with sequential growth and differentiation factors.

Co-culture assembly. Co-cultures were established by seeding GFP-labeled HCB-GICs onto mature organoids, as previously described by Pedrosa et al. (2023) [16]. Cultures were maintained for 20 days, with periodic monitoring of GIC infiltration using an Olympus BX41 microscope equipped with a GFP filter.

4.2. Molecular Profiling of HCB-GICs

DNA extraction and analysis. Genomic DNA was extracted from primary cultures by using the Blood and Cell Culture DNA Mini kit (Qiagen 13323, Hilden, Germany) and from tumor tissues by using the QIAamp DNA FFPE Tissue Kit (Qiagen, 56404, Hilden, Germany). Total DNA was quantified with the Invitrogen Qubit 4 fluorometer. Concentration and purity of DNA were determined by measuring the absorbance (A260/280) of the sample with the NanoDrop ND-1000 Spectrophotometer (Thermo Fisher Scientific, Waltham, MA, USA).

Genetic assessment. The OncoScan assays (Applied Biosystems™, Thermo Fisher Scientific) were used for genetic comparison between HCB-GICs and their respective tumours. Analysis was performed with Chromosome Analysis Suite Version 4.3 (Thermo Fisher Scientific).

4.3. Cellular Components of Human Brain Organoids and GICs Co-Cultures

The cellular composition and spatial distribution within the brain organoids were assessed by double immunofluorescence and by flow cytometry analysis of CD44 and CD133 expression in GFP^+ cells (see Supplementary Materials).

4.4. 5-ALA/PDT Testing In Vitro: HCB-GICs & Brain-Organoid Co-Cultures

The in vitro 5-ALA PDT experiments were conducted using twin 96-well plates: one plate for irradiation (1.2 J/cm^2) and a paired non-irradiated control, as previously described by our group [16]. Each plate was split into two treatment groups—5-ALA (50 µg/mL) and vehicle control—each containing at least six replicates of (1) brain organoids, (2) HCB-GIC tumorspheres alone, and (3) co-cultures of organoids with HCB-GICs. To evaluate the four GIC lines, two sets of paired plates were used: one set for HCB-GIC1 and HCB-GIC4, and another for HCB-GIC19 and HCB-GIC20. After 24 h of 5-ALA exposure, one plate from each pair was irradiated for 15 min (total dose 1.2 J/cm^2) while its twin remained non-irradiated.

4.5. Determination of PDT Efficacy In Vitro

In vitro efficacy of 5-ALA PDT was evaluated using three complementary assays. Fluorescence of HCB-GICs expressing GFP was measured (excitation 485 nm, emission 530 nm) from the bottom of each well (lid in place) at 12 randomized positions per well using an Infinite M Plex plate reader (Tecan, Trading AG, Switzerland). Readings were acquired immediately post-irradiation (t = 0) and at 24 h (t = 1) and 72 h (t = 2), and viability loss was quantified as the ratio of GFP signal at t = 1 or t = 2 relative to t = 0, with representative high-resolution images captured under GFP filter on an EVOS M7000 (Invitrogen, Thermo Scientific). Concurrently, 25 µL of supernatant was collected at each time point to measure lactate dehydrogenase activity (LDH Cytotoxicity Assay) (Promega, Madison, WI, USA). The amount of LDH released into the medium was used as an indicator of cell death. Differential LDH levels between time points were calculated to assess changes in cytotoxicity.

Apoptotic cell death was determined by TUNEL staining. Co-cultures were fixed and stained using the Click-iT Plus TUNEL kit (Invitrogen, C10618, Waltham, MA, USA) with Alexa Fluor 594, followed by DAPI counterstaining; fluorescent images were acquired on a Nikon Eclipse Ni-E microscope (Izasa Scientific, Barcelona, Spain) and analyzed with ImageJ 1.54g.

4.6. Animal Subjects

All experiments involving animals were approved by the Ethics Committee of our University (PNT 2090206 DOC/002). All methods were carried out in accordance with the institutional animal care guidelines and relevant regulations under the protocol CEEA 421/22, which were controlled periodically during the experimental process.

NOD/SCID/gamma(c)(null) mice (NSG), which are double homozygous for the severe combined immunodeficiency (SCID) mutation and interleukin-2Rgamma (IL-2Rgamma) allelic mutation (gamma(c)(null)), were used for the in vivo experiments.

4.7. 5-ALA/PDT Testing In Vivo: HCB-GICs Human-Brain-Organoid Xenograft

Details on the generation of the HCB-GICs brain-organoid xenograft in the renal subcapsular space of immunosuppressed mice can be found in Supplementary Materials. After the engraftment, animals were kept alive for 40 days to allow for tumoral/organoid growth and infiltration prior to PDT testing. Specific details in the PDT procedure can be found in Supplementary Materials.

Selected animals were administered 5-ALA (Gliolan, 5-aminolevulinic acid hydrochloride) orally at 100 mg/kg and protected from lighting. After 4 h, 5ALA/PDT was delivered to one of the kidneys (right side), at a wavelength of 635 nm and a power of 5 mW for 10 min. In each mouse, the contralateral kidney (left side) was left untreated as a control. The procedure was carried out under general anesthesia with isoflurane 4% induction and 2% maintenance, while oxygenation was kept at a FiO2 of 30% during the whole duration of the experiment. A custom-made integrated irradiation system was used for PDT (Universitat Politecnica de Catalunya, UPC, Barcelona, Spain). The instrument was specifically designed to guarantee that the light emitted was directed only to the area of interest. This was achieved by an adjustable diaphragm coupled with the light-emitting diode.

Before starting the irradiation period, the selected kidney was externalized by reopening the retroperitoneal incision used during the first intervention for tumor engraftment. The opening of the diaphragm was manually adjusted to cover the surface of the kidney, making sure the lightened area was restricted to the kidney. The contralateral kidney used as a control (and other surrounding tissues) was protected from the light source throughout the whole duration of the PDT delivery. For this, the control kidney was kept in

the retroperitoneal space, and the area of light exposure was restricted to the area occupied by the contralateral externalized kidney.

After the treatment, animals were kept alive for seven days after sacrifice and kidney removal.

IVIS Imaging System (Caliper, Hopkinton, MA, USA) was used for ex vivo measurement of the relative fluorescent units (RFU) of GFP-positive cells as indicative of tumor burden. Emission of RFU on treated kidneys in comparison with the contralateral untreated controls was evaluated. Renal tissues were then fixed and preserved.

4.8. Statistical Analysis

Data are presented as mean ± SEM. Two-tailed Student's t test or ANOVA were used as appropriate using GraphPad Prism (version 8.0.2, Insightful science, CA, USA). A Bonferroni post-hoc test was performed to compare the replicate means. Statistical significance was denoted as: * $p < 0.05$, ** $p < 0.01$, and *** $p < 0.001$.

Additional information on the methodology can be found in Appendices A–D.

5. Conclusions

We describe an in vitro and in vivo model of human glioblastoma based on a co-culture allowing the infiltration of glioblastoma-initiating cells into brain organoids, which can be studied ex vivo or transferred to immunosuppressed mice as a xenograft. Both strategies were constructed upon patient-derived tumoral cells and demonstrated to capture the genetic heterogeneity of glioblastoma, providing a realistic and personalized model for therapy testing. We successfully applied the model to test the effects of 5-ALA-mediated PDT both in vitro and in vivo and describe the differences in the treatment effects according to the genetic and phenotypic properties of each cell line. These results may be determinant to understand the role of the microenvironment in GB biology and treatment response.

Supplementary Materials: The following supporting information can be downloaded at: https://www.mdpi.com/article/10.3390/ijms26188889/s1.

Author Contributions: Conceptualization, A.M., L.P., À.S.J. and J.J.G.S.; methodology, A.M., L.P., A.S., À.S.J. and J.J.G.S.; software, D.D.; validation, all authors; formal analysis, A.M., D.D., G.C., I.A., À.S.J. and J.J.G.S.; investigation, A.M., D.D., C.B., M.M. and F.S.; resources, A.S., M.M.-T. and M.C.; data curation, A.M., D.D., G.A.C., I.A., A.F., G.C., E.P. and A.S.; writing—original draft preparation, A.M. and D.D.; writing—review and editing, all authors; visualization, all authors; supervision, À.S.J. and J.J.G.S.; project administration, M.M.-T., M.C., À.S.J. and J.J.G.S.; funding acquisition, M.M.-T., M.C., À.S.J. and J.J.G.S. All authors have read and agreed to the published version of the manuscript.

Funding: The authors acknowledge the financial support from Laboratorios Gebro Pharma S.A. to set up this project (LGP Study code: LGP17-19). L.P. and D.D. acknowledge AECC (Spanish Association Against Cancer. Project GCTRA16015SEDA). This work was supported in part by 2021 SGR 00560 (GRC) Generalitat de Catalunya; economic support from CERCA Programme/Generalitat de Catalunya, Fundació Internacional Josep Carreras. AS acknowledge her financial support from the grant PID2022-137672NB-I00 funded by MCIN/AEI/10.13039/501100011033 and by the ERDF A way of making Europe, the grant PDC 2022-133826-100 funded by MCIN/AEI/10.13039/501100011033 and by the European Union Next Generation EU/PRTR, the grant CNS2023-144709 funded by MCIN/AEI/10.13039/501100011033 and by the European Union Next Generation EU/PRTR and the Catalan Government (2021SGR00453 and 2021-SGR-01423).

Institutional Review Board Statement: The animal study protocol was approved by the Institutional Review Board (or Ethics Committee) of Universitat de Barcelona (protocol code PNT 2090206 DOC/002 and date of approval 6th June 2023). The participation of patients in this study was ap-proved by the Institutional Ethics Committee of Hospital Clínic Barcelona (pro-tocol code HCB/2020/0137 and date of approval 27th February 2020).

Informed Consent Statement: Informed consent was obtained from all subjects involved in the study.

Data Availability Statement: Data may be shared with other investigators upon reasonable request and provided the approval of the Institutional Ethics Committee.

Conflicts of Interest: The authors declare that this study received funding from Laboratorios Gebro Pharma S.A, along with other public institutions. The funder remained independent throughout the execution of the study; it had no role in the design of the study; neither in the collection and analysis, nor in the interpretation of data; in the writing of the manuscript; or in the decision to publish the results. The authors Marta Muñoz-Tudurí and Marc Centellas were employed by the company La-boratorios Gebro Pharma S.A. All other authors have no conflicts of interest to declare.

Abbreviations

The following abbreviations are used in this manuscript:

GB	Glioblastoma
PDT	Photodynamic therapy
GIC	Glioblastoma initiating cells
CNS	Central nervous system
5-ALA	5-aminolevulinic acid
PDD	Photodynamic diagnosis
PS	Photosensitizer
PFS	Progression-free survival
CNA	Copy number alterations
cnLOH	Copy neutral loss of heterozygosity
RFU	Relative fluorescence units
MDM1/2	Mouse double-minute 1 and 2
GFAP	Glial fibrillary acid protein
TUJ1	Tubulin betta class 3
CD44	Cluster of differentiation-44
CD133	Cluster of differentiation-133
MGMT	O6-methylguanine-DNA methyltransferase
CDK4/6	Cyclin-dependent kinase 4 and 6
CDKN2A/B	Cyclin-dependent kinase inhibitor 2A/B
CCND2	Cyclin D2
Rb	Retinoblastoma protein
PIK3CA	Phosphatidylinositol-4,5-bisphosphate 3-kinase catalytic subunit alpha
PIK3R	Phosphoinositide-3-kinase regulator
PTEN	Phosphatase and tensin homolog
EGFR	Epidermal growth factor receptor
PDGFR1	Platelet derived growth factor receptor 1
NF1	Neurofibromin
SOX2	Sex determining region Y-box 2
LDH	Lactate Dehydrogenase
NSG	NOD scid gamma mouse
TUNEL	Terminal deoxynucleotidyl transferase dUTP Nick End Labeling assay
WHO	World health organization
HCB	Hospital Clínic de Barcelona

Appendix A. Patient-Derived HCB-GICs: Clinical Features

HCB-GICs were obtained from a series of four patients surgically treated at our institution. According to the Pathology Department and based on the WHO Classification of Tumors of the Central Nervous System criteria (5th edition, 2021), all four patients were diagnosed with MGMT-methylated IDH wild-type grade 4 gliomas.

These patients were part of a bigger dataset including detailed clinical records of patients undergoing various treatments for brain tumors. The codified registry was conducted between January 2021 and December 202, and contains information about diagnostic timelines, progression patterns, and survival outcomes. Progression-free survival (PFS) intervals varied widely between the four subjects, from early progression (e.g., 95 days) to prolonged intervals (e.g., 795 days). Progression types are categorized into pseudoprogression and genuine progression, supporting nuanced survival analyses. Treatment regimens also varied, encompassing monotherapies, combined modalities such as radiotherapy with temozolomide, and the use of bevacizumab in recurrent cases, with some patients undergoing complete surgical resections. Outcome data include overall survival (OS) times, with durations of up to 901 days, and clearly documented death dates and follow-up records, ensuring accurate survival endpoints. Recurrence was noted in several cases, often linked to progression events, and follow-up dates span from 2021 to 2024, allowing for robust longitudinal analyses.

Histological analysis revealed a predominant astroglial differentiation (Supplementary Figure S1), cell morphology varied between cases, as well as intratumorally, but ranged from cells with scarce cytoplasm to large gemistocytic and even epithelioid morphology. Mitosis was frequent, in addition to necrosis and microvascular proliferation. All cases were IDH1 non-mutated by immunohistochemistry and IDH1 and IDH2 sequencing. ATRX nuclear expression was retained in all assessable cases, and two cases had TERT promoter mutation c.-124 C > T. There was no discernible correlation between the age of patients and the proliferation index using Ki67. It was observed that the youngest patient, aged 51 years, and the oldest patient, aged 77 years, exhibited the highest levels of Ki67 staining, while patients aged 55 and 60 showed levels ranging from 15 to 20% of Ki67, respectively. Only one had an immunohistochemical p53 pattern compatible with mutation, with a proliferation index of 50%. Three of the samples originated from temporal tumors, while only one derived from a frontal tumor.

From the resected tumors from these patients, we obtained four different HCB-GICs (following the described protocol, Figure 1A): HCB-GIC1, HCB-GIC4, HCB-GIC19 and HCB-GIC20, with similar growth ratio, but differing in their phenotype.

About 15–20 days after the isolation, we observed the formation of tumorspheres. In fact, HCB-GIC19 and HCB-GIC20 formed tumorspheres, in contrast to HCB-GIC4 that showed the ability to grow in adhesion with a characteristic spicular cytoplasmic neural-like extension (Figure 1B and Supplementary Figure S2).

Since the sole formation of tumorspheres does not provide, per se, a demonstration of the presence of GSCs, the stem nature of the HCB-GICs primary cultures was further evident by evaluating the expression of specific markers of stemness and invasion as CD133 and CD44, respectively, using flow cytometry.

CD133, a membrane-bound glycoprotein found on the surface of stem cells, showed variable expression among HCB-GICs (Figure 1C). Whereas less than 20% of cells were positive for CD133 in HCB-GIC1 and HCB-GIC19, over 70% of HCB-GIC4 and HCB-GIC20 cells expressed CD133 (Bonferroni's multiple comparison test, $p < 0.0001$). No significant differences in CD44 expression were observed between the cell lines (Bonferroni's multiple comparison test, $p = 0.384$), as 90% of cells across all four HCB-GICs expressed this membrane receptor (Figure 1C). CD44 is known to promote both invasion and proliferation of tumor cells through various signaling pathways, contributing to the highly invasive and radio-chemotherapy-resistant nature of GICs. These findings confirmed the highly aggressive phenotype of all HCB-GICs.

Appendix B. Primary Cell Lines Establishment

With written consent from patients and in accordance with the University of Barcelona guidelines, glioblastoma initiating cells (GICs) were obtained from successive glioblastoma biopsies as previously described [17]: tumors were collected immediately after resection in a sterile container with RPMI-1640 media (Gibco, 21875-034, Bleiswijk, The Netherlands) on ice, and incubated 37 °C for 45 min, under 1400 rpm stirring with enzymatic tissue dissociation solution (Tumor Dissociation Kit, Miltenyi Biotec, 130-095-929, Auburn, AL USA). After supernatant filtration, cells were pelleted at 400× *g* 10 min and resuspended in complete neurobasal (NB medium). The tumorspheres formed after 2–3 weeks were collected, pelleted, disaggregated and transferred into new flasks with fresh supplemented media. Partial media changes were performed every 3–4 days until progressively raised to a complete Neural Stem Cell (NSC) medium (Figure 1A and Supplementary Materials for more details). Finally, to allow the follow-up of Hospital Clinic Barcelona-GICs (HCB-GICs) in the organoid co-cultures, HCB-GICs were infected with lentiviral vectors carrying green fluorescent protein (GFP).

Cerebral organoids. Induced pluripotent stem cells (iPSCs) were first cultured on Geltrex and then transferred to low-adherence U-bottom 96-well plates, where they were grown in spheroid starter media containing specific inhibitors and supplements [18]. Over the course of several weeks, the media gradually changed and supplemented with growth factors like bFGF and EGF to promote spheroid development. By day 20, spheroids were moved to ultra-low attachment 96-well plates for further culture, and neural differentiation began between days 27 and 41 using a medium supplemented with BDNF and NT-3. From day 41 onwards, the spheroids were maintained for the generation of the assembled culture with HCP-GICs.

HCB-GIC-Organoid Co-culture. The protocol of co-culture was performed as previously described [16]: co-cultures were initiated on day 47 of organoid differentiation by plating 2 × 10^3 cells per well, each containing a single organoid. Over the next 20 days, cultures were monitored using an OlympusBX41 microscope with a GFP filter to track their evolution and infiltration into the brain organoid. This evaluation was conducted prior to the implantation of the co-cultures into the renal capsules of NSG mice.

Appendix C.

Appendix C.1. DNA Extraction and Analysis

Genomic DNA was extracted from primary cultures by using the Blood and Cell Culture DNA Mini kit (Qiagen 13323, Hilden, Germany) and from tumor tissues by using the QIAamp DNA FFPE Tissue Kit (Qiagen, 56404, Hilden, Germany). The manufacturer's instructions were followed and after the protein removal, the samples were placed into a spin column system to concentrate DNA before elution. The total DNA from each sample was quantified using the Invitrogen Qubit 4 fluorometer from Thermo Fisher. The concentration and the purity of the extracted DNA were determined by measuring the absorbance (A260/280) of the sample with the NanoDrop ND-1000 Spectrophotometer (Thermo Fisher Scientific, Waltham, MA, USA).

Appendix C.2. Genetic Assessment

The OncoScan assays (Applied Biosystems™, Thermo Fisher Scientific), based on Molecular Inversion Probe (MIP) technology, are proven for identifying CN (copy numbers) alterations, and copy-neutral loss of heterozygosity (cnLOH) was used for genetic comparison between HCB-GICs and their respective tumors. This assay has been shown to perform well with highly degraded DNA, such as that derived from formalin-fixed,

paraffin-embedded (FFPE) tumor samples of various ages, and with low amounts of DNA starting material.

The analysis was performed with Chromosome Analysis Suite Version 4.3 (Thermo Fisher Scientific). All samples met quality control (QC) thresholds and were included in the analysis. Data was analyzed using annotations of genome version GRCh38 (hg38). Detailed visual data analysis was performed in all samples in addition to software-reported alterations. Only copy number (CN) segments with a minimum genomic size of 100 Kb and with at least 20 SNP/CN-altered markers cnLOH $\geq$ 5 Mb were reported. Furthermore, inborn genetic abnormalities were excluded by comparing findings with control Databases. SNP array data have been deposited in the GEO database under accession number GSE279049.

Appendix C.3. Double Immunofluorescence (IF) Analysis

Whole organoids were fixed with 4% paraformaldehyde (PFA) for 20 min, washed with PBS prior to overnight (O/N) incubation in 30% sucrose (weight/volume) at 4 °C and embedded in Tissue-Tek® O.C.T.™. (Sakura Finetek, #127217, Torrance, CA, USA). Cryosections of 12 µm were obtained with Leica CM1950 cryostat (Leica Biosystems, Barcelona, Spain) and stored at −80 °C for long-term storage. Sections were then allowed to equilibrate at room temperature, encircled with the hydrophobic super PAN pen (Sigma-Aldrich, Z672548-1EA, Madrid, Spain) and dried for 5 min. The sections were permeabilized in 0,4% Triton X-100 in PBS, rinsed and blocked in 5% goat serum (Abcam, ab7481, Cambridge, UK) at room temperature, and then incubated with the primary antibodies for 1.5 h in a humidified chamber. Slides were then washed 3 times in 0.1% Tween PBS and incubated with secondary antibodies (Supplementary Table S1). Sections were mounted and nuclei stained in Fluoromount DAPI (SouthernBiotech, 0100-20, Birmingham, AL, USA).

Images were captured at 10×, 20× and 40× magnifications, using Nikon Eclipse Ni (Izasa Scientific, Barcelona, Spain) fluorescence microscope and analyzed using ImageJ 1.54 g and GraphPad Prism. Average protein expression of IF images was assessed by quantifying positive cells in five different areas of both control and PDT tissues at 40×.

Appendix C.4. TUNEL Analysis

Terminal deoxynucleotidyl transferase (TdT)-mediated dUTP nick-end labelling (TUNEL) assay (Click-iT Plus TUNEL, Invitrogen, C10618, Waltham, MA, USA) was used with Alexa Fluor 594 dye to in situ analyze apoptotic cells in tumor-organoid co-cultures. Briefly, tissue cryosections were air-dried at room temperature for 5 min, and permeabilized with proteinase K before performing the TdT 1 h reaction at 37 °C. Then, the samples were incubated with Alexa Fluor 594, 30 min, protected from light.

Fluoromount DAPI was used as a nuclear counterstain. Images were taken with a Nikon Eclipse Ni-E (Izasa Scientific, Barcelona, Spain) fluorescence microscope using standard fluorescein excitation and emission filters. Images were analyzed using ImageJ 1.54g and GraphPad Prism.

Appendix C.5. Flow Cytometry

The expression profiles of CD44 and CD133 in GFP-positive cells were analyzed by flow cytometry. Three independent experiments were carried out for all cell lines. Briefly, 106 cells were washed with 1% BSA in PBS (FC buffer) and centrifuged at 2000 rpm 5 min. Cell pellets resuspended in 100 µL of FC buffer were incubated with the appropriate antibody, either PE-conjugated 1/100 anti-CD133 (Milteny Biotech, 130-111-079, Bergisch, Germany) or 1/25 anti-CD44 (BD Pharmingen, 550392,Spain) followed by secondary AF594 at 1/1000 (Invitrogen, A11005) 30 min on ice in the dark. The analysis was carried out in an

LRSFortessa 5L flow cytometer (BD Biosciences, Madrid, Spain). Unstained cells served as negative controls.

Appendix D.

Appendix D.1. In Vivo Model of Renal Subcapsular HCB-GICs Brain-Organoid Engraftment

Mice were housed in an animal room with strict humidity (50–60%) and temperature (22–24 °C) control, under a 12-h day/night cycle. Groups of three animals were housed in plastic cages with free access to standard food and tap water.

Engraftment procedure. First, animals were anesthetized with isoflurane 4% and maintained with an inhalation dose of 2%. After disinfecting the surgical site, the retroperitoneum was accessed through a 1.5–2 cm midline dorsal incision. Through a blunt dissection of the paraspinal muscles, the left kidney was identified and carefully exteriorized, preserving its hilum. The renal capsule was incised for 2–4 mm with an ophthalmic knife and the subcapsular space was delicately dissected. Using a glass pipette with a blunt tip, four organoids/GICs were inoculated in the subcapsular space. The kidney was then reintroduced into the retroperitoneal space. The same procedure was then repeated in the right kidney. The wound was closed with surgical staples (Supplementary Figure S11). Animals were maintained under close postoperative surveillance for three days. They were kept alive for 40 days to allow for tumoral/organoid engraftment prior to PDT.

Appendix D.2. In Vivo 5-ALA/PDT Treatment

On day +40 after organoid/tumor engraftment in the renal subcapsular space of NSG mice, 5ALA/PDT was delivered to one of the kidneys (right side). In each mouse, the contralateral kidney (left side) was left untreated as a control.

Before proceeding to PDT in vivo treatment, 5-ALA uptake, metabolism, and optimal time window for the use of oral 5-ALA as the PDT substrate was explored (Supplementary Figure S8). These experiments indicated that fluorescence was maximal in selected tissues 4 h after administration of 5-ALA 100 mg/kg, confirming this optimal time window for irradiation of the renal engraftment with the integrated spectrometer and light source system (Supplementary Figure S9).

A custom-made integrated irradiation system was used for PDT (Universitat Politecnica de Catalunya, UPC, Barcelona, Spain). The instrument with an LED M625L4 (SN M00928350) was regulated by a power supply LEDD1B (SN M00949558), T-Cube LED Driver (Thorlabs Inc. GmbH). The spectrometer CAS140D157U1B (SN 303014423) from Instrument Systems, GmbH, has been calibrated with standards from the Institute of Standards and Technology (NIST) and Physikalisch-Technische Bundesanstalt (PTB).

First, animals were administered 5-ALA (Gliolan, 5-aminolevulinic acid hydrochloride) orally through a nasogastric canula, at a dose of 100 mg/kg. After administration, they were protected from lighting and 4 h later, the PDT procedure began. Animals were anesthetized with 4% isoflurane and maintained with a 2% inhalation dose. The midline dorsal incision was reopened, and the right kidney was externalized as described above. The irradiation probe was placed 3 cm above the surface of the kidney to attain the optimal lighting exposure as specified by the manufacturer. The light diaphragm available in the irradiation device was applied to include the whole kidney and minimize the exposure of adjacent structures. The right kidney was irradiated at a wavelength of 635 nm and a power of 5 mW for 10 min. After PDT, the kidney was reintroduced in the retroperitoneal cavity and the wound was again closed. The left (control) kidney was kept in the retroperitoneal space, protected from the light.

Animals were maintained under close postoperative surveillance for three days. They were kept alive for seven days after sacrifice and kidney removal.

IVIS Imaging System (Caliper, Hopkinton, MA) was used for ex vivo measurement of the relative fluorescent units (RFU) of GFP-positive cells as indicative of tumor burden. Emission of RFU on treated kidneys in comparison with the contralateral untreated controls was evaluated.

Renal tissues were then preserved as described before: first fixed 4% paraformaldehyde (PFA) for 20 min, washed with PBS prior to overnight incubation in 30% sucrose (weight/volume) at 4 °C and embedded in OCT.

References

1. Sanai, N.; Polley, M.Y.; McDermott, M.W.; Parsa, A.T.; Berger, M.S. An extent of resection threshold for newly diagnosed glioblastomas. *J. Neurosurg.* **2011**, *115*, 3–8. [CrossRef] [PubMed]
2. Louis, D.N.; Perry, A.; Wesseling, P.; Brat, D.J.; Cree, I.A.; Figarella-Branger, D.; Hawkins, C.; Ng, H.K.; Pfister, S.M.; Reifenberger, G.; et al. The 2021 WHO classification of tumors of the central nervous system: A summary. *Neuro-Oncology* **2021**, *23*, 1231–1251. [CrossRef]
3. Louis, D.N.; Perry, A.; Reifenberger, G.; Von Deimling, A.; Figarella-Branger, D.; Cavenee, W.K.; Ohgaki, H.; Wiestler, O.D.; Kleihues, P.; Ellison, D.W. The 2016 World Health Organization Classification of Tumors of the Central Nervous System: A summary. *Acta Neuropathol.* **2016**, *131*, 803–820. [CrossRef]
4. Horbinski, C.; Berger, T.; Packer, R.J.; Wen, P.Y. Clinical implications of the 2021 edition of the WHO classification of central nervous system tumours. *Nat. Rev. Neurol.* **2022**, *18*, 515–529. [CrossRef]
5. Perez, A.; Huse, J.T. The Evolving Classification of Diffuse Gliomas: World Health Organization Updates for 2021. *Curr. Neurol. Neurosci. Rep.* **2021**, *21*, 67. [CrossRef]
6. Diksin, M.; Smith, S.J.; Rahman, R. The Molecular and Phenotypic Basis of the Glioma Invasive Perivascular Niche. *Int. J. Mol. Sci.* **2017**, *18*, 2342. [CrossRef]
7. Quail, D.F.; Joyce, J.A. The Microenvironmental Landscape of Brain Tumors. *Cancer Cell* **2017**, *31*, 326–341. [CrossRef] [PubMed]
8. Mosteiro, A.; Pedrosa, L.; Ferrés, A.; Diao, D.; Sierra, À.; González, J.J. The Vascular Microenvironment in Glioblastoma: A Comprehensive Review. *Biomedicines* **2022**, *10*, 1285. [CrossRef]
9. Wang, J.; Cazzato, E.; Ladewig, E.; Frattini, V.; Rosenbloom, D.I.S.; Zairis, S.; Abate, F.; Liu, Z.; Elliott, O.; Shin, Y.-J.; et al. Clonal evolution of glioblastoma under therapy. *Nat. Genet.* **2016**, *48*, 768–776. [CrossRef] [PubMed]
10. Turnquist, C.; Beck, J.A.; Horikawa, I.; Obiorah, I.E.; Von Muhlinen, N.; Vojtesek, B.; Lane, D.P.; Grunseich, C.; Chahine, J.J.; Ames, H.M.; et al. Radiation-induced astrocyte senescence is rescued by Δ133p53. *Neuro-Oncology* **2019**, *21*, 474–485. [CrossRef]
11. Krammer, B.; Plaetzer, K. ALA and its clinical impact, from bench to bedside. *Photochem. Photobiol. Sci.* **2008**, *7*, 283–289. [CrossRef] [PubMed]
12. Kennedy, J.C.; Pottier, R.H. Endogenous protoporphyrin IX, a clinically useful photosensitizer for photodynamic therapy. *J. Photochem. Photobiol. B Biol.* **1992**, *14*, 275–292. [CrossRef]
13. Aldape, K.; Brindle, K.M.; Chesler, L.; Chopra, R.; Gajjar, A.; Gilbert, M.R.; Gottardo, N.; Gutmann, D.H.; Hargrave, D.; Holland, E.C.; et al. Challenges to curing primary brain tumours. *Nat. Rev. Clin. Oncol.* **2019**, *16*, 509–520. [CrossRef]
14. Cramer, S.W.; Chen, C.C. Photodynamic Therapy for the Treatment of Glioblastoma. *Front. Surg.* **2019**, *6*, 81. [CrossRef] [PubMed]
15. Vasilev, A.; Sofi, R.; Rahman, R.; Smith, S.J.; Teschemacher, A.G.; Kasparov, S. Using Light for Therapy of Glioblastoma Multiforme (GBM). *Brain Sci.* **2020**, *10*, 75. [CrossRef]
16. Pedrosa, L.; Bedia, C.; Diao, D.; Mosteiro, A.; Ferrés, A.; Stanzani, E.; Martínez-Soler, F.; Tortosa, A.; Pineda, E.; Aldecoa, I.; et al. Preclinical Studies with Glioblastoma Brain Organoid Co-Cultures Show Efficient 5-ALA Photodynamic Therapy. *Cells* **2023**, *12*, 1125. [CrossRef]
17. Van de Mark, D.; Kong, D.; Loncarek, J.; Stearns, T.; Chang, F. MDM1 is a microtubule-binding protein that negatively regulates centriole duplication. *Mol. Biol. Cell* **2015**, *26*, 3788–3802. [CrossRef] [PubMed]
18. Kim, Y.; Varn, F.S.; Park, S.-H.; Yoon, B.W.; Park, H.R.; Lee, C.; Verhaak, R.G.W.; Paek, S.H. Perspective of mesenchymal transformation in glioblastoma. *Acta Neuropathol. Commun.* **2021**, *9*, 50. [CrossRef]
19. Lee, J.; Kotliarova, S.; Kotliarov, Y.; Li, A.; Su, Q.; Donin, N.M.; Pastorino, S.; Purow, B.W.; Christopher, N.; Zhang, W.; et al. Tumor stem cells derived from glioblastomas cultured in bFGF and EGF more closely mirror the phenotype and genotype of primary tumors than do serum-cultured cell lines. *Cancer Cell* **2006**, *9*, 391–403. [CrossRef]
20. Bao, S.; Wu, Q.; McLendon, R.E.; Hao, Y.; Shi, Q.; Hjelmeland, A.B.; Dewhirst, M.W.; Bigner, D.D.; Rich, J.N. Glioma stem cells promote radioresistance by preferential activation of the DNA damage response. *Nature* **2006**, *444*, 756–760. [CrossRef]
21. da Silva, B.; Mathew, R.K.; Polson, E.S.; Williams, J.; Wurdak, H. Spontaneous Glioblastoma Spheroid Infiltration of Early-Stage Cerebral Organoids Models Brain Tumor Invasion. *SLAS Discov. Adv. Sci. Drug Discov.* **2018**, *23*, 862–868. [CrossRef]

22. Sloan, A.R.; Silver, D.J.; Kint, S.; Gallo, M.; Lathia, J.D. Cancer stem cell hypothesis 2.0 in glioblastoma: Where are we now and where are we going? *Neuro-Oncology* **2024**, *26*, 785–795. [CrossRef]
23. Verhaak, R.G.W.; Hoadley, K.A.; Purdom, E.; Wang, V.; Wilkerson, M.D.; Miller, C.R.; Ding, L.; Golub, T.; Jill, P.; Alexe, G.; et al. Integrated Genomic Analysis Identifies Clinically Relevant Subtypes of Glioblastoma Characterized by Abnormalities in PDGFRA, IDH1, EGFR, and NF1. *Cancer Cell* **2010**, *17*, 98–110. [CrossRef] [PubMed]
24. Pavon, L.F.; Sibov, T.T.; de Oliveira, D.M.; Marti, L.C.; Cabral, F.R.; de Souza, J.G.; Boufleur, P.; Malheiros, S.M.; Neto, M.A.d.P.; da Cruz, E.F.; et al. Mesenchymal stem cell-like properties of CD133+ glioblastoma initiating cells. *Oncotarget* **2016**, *7*, 40546–40557. [CrossRef]
25. Inoue, A.; Ohnishi, T.; Nishikawa, M.; Ohtsuka, Y.; Kusakabe, K.; Yano, H.; Tanaka, J.; Kunieda, T.A. Narrative Review on CD44's Role in Glioblastoma Invasion, Proliferation, and Tumor Recurrence. *Cancers* **2023**, *15*, 4898. [CrossRef]
26. Bian, S.; Repic, M.; Guo, Z.; Kavirayani, A.; Burkard, T.; Bagley, J.A.; Krauditsch, C.; Knoblich, J.A. Author Correction: Genetically engineered cerebral organoids model brain tumor formation. *Nat. Methods* **2018**, *15*, 748, Correction in *Nat. Methods* **2018**, *15*, 631–639. [CrossRef] [PubMed]
27. Vermandel, M.; Quidet, M.; Vignion-Dewalle, A.-S.; Leroy, H.-A.; Leroux, B.; Mordon, S.; Reyns, N. Comparison of different treatment schemes in 5-ALA interstitial photodynamic therapy for high-grade glioma in a preclinical model: An MRI study. *Photodiagn. Photodyn. Ther.* **2019**, *25*, 166–176. [CrossRef]
28. Curnow, A.; Haller, J.; Bown, S. Oxygen monitoring during 5-aminolaevulinic acid induced photodynamic therapy in normal rat colon. *J. Photochem. Photobiol. B Biol.* **2000**, *58*, 149–155. [CrossRef] [PubMed]
29. Fontana, A.O.; Piffaretti, D.; Marchi, F.; Burgio, F.; Faia-Torres, A.B.; Paganetti, P.; Pinton, S.; Pieles, U.; Reinert, M. Epithelial growth factor receptor expression influences 5-ALA induced glioblastoma fluorescence. *J. Neuro-Oncol.* **2017**, *133*, 497–507. [CrossRef]
30. Ghantasala, S.; Bhat, A.; Agarwal, U.; Biswas, D.; Bhattarai, P.; Epari, S.; Moiyadi, A.; Srivastava, S. Deep proteome investigation of high-grade gliomas reveals heterogeneity driving differential metabolism of 5-aminolevulinic acid. *Neuro-Oncol. Adv.* **2023**, *5*, vdad065. [CrossRef]
31. Pantazopoulou, V.; Jeannot, P.; Rosberg, R.; Berg, T.J.; Pietras, A. Hypoxia-Induced Reactivity of Tumor-Associated Astrocytes Affects Glioma Cell Properties. *Cells* **2021**, *10*, 613. [CrossRef] [PubMed]
32. Escartin, C.; Galea, E.; Lakatos, A.; O'cAllaghan, J.P.; Petzold, G.C.; Serrano-Pozo, A.; Steinhäuser, C.; Volterra, A.; Carmignoto, G.; Agarwal, A.; et al. Reactive astrocyte nomenclature, definitions, and future directions. *Nat. Neurosci.* **2021**, *24*, 312–325. [CrossRef] [PubMed]
33. Lawrence, J.M.; Schardien, K.; Wigdahl, B.; Nonnemacher, M.R. Roles of neuropathology-associated reactive astrocytes: A systematic review. *Acta Neuropathol. Commun.* **2023**, *11*, 42. [CrossRef]
34. Perelroizen, R.; Philosof, B.; Budick-Harmelin, N.; Chernobylsky, T.; Ron, A.; Katzir, R.; Shimon, D.; Tessler, A.; Adir, O.; Gaoni-Yogev, A.; et al. Astrocyte immunometabolic regulation of the tumour microenvironment drives glioblastoma pathogenicity. *Brain* **2022**, *145*, 3288–3307. [CrossRef]
35. Frenster, J.D.; Placantonakis, D.G. Establishing Primary Human Glioblastoma Tumorsphere Cultures from Operative Specimens. *Methods Mol. Biol.* **2018**, *1741*, 63–69. [CrossRef]
36. Han, J.-h.; Yoon, J.S.; Chang, D.-Y.; Cho, K.G.; Lim, J.; Kim, S.-S.; Suh-Kim, H. CXCR4-STAT3 Axis Plays a Role in Tumor Cell Infiltration in an Orthotopic Mouse Glioblastoma Model. *Mol. Cells* **2020**, *43*, 539–550. [CrossRef] [PubMed]

Disclaimer/Publisher's Note: The statements, opinions and data contained in all publications are solely those of the individual author(s) and contributor(s) and not of MDPI and/or the editor(s). MDPI and/or the editor(s) disclaim responsibility for any injury to people or property resulting from any ideas, methods, instructions or products referred to in the content.